Journal of Materials Chemistry A

PAPER

View Article Online
View Journal | View Issue

Cite this: J. Mater. Chem. A, 2019, 7, 16516

Hybrid electrolyte enables safe and practical 5 V $LiNi_{0.5}Mn_{1.5}O_4$ batteries†

Purna Chandra Rath,[a] Chia-Jung Wu,[b] Jagabandhu Patra,[ac] Ju Li,[*d] Tai-Chou Lee,[b] Ting-Ju Yeh[e] and Jeng Kuei Chang[*ac]

Received 20th April 2019
Accepted 18th June 2019

DOI: 10.1039/c9ta04147h

rsc.li/materials-a

Bis(trifluoromethylsulfonyl)imide (TFSI)-based ionic liquid (IL) has high thermal and electrochemical stability, but it is not an ideal battery electrolyte due to the poor rate capability of cells that use it, problematic anode compatibility, and high cost. The incorporation of a carbonate solvent could mitigate these problems, but it would also lead to serious Al current collector corrosion at high potential. This long-existing problem is overcome in this study by modulating the LiTFSI concentration and IL/carbonate ratio in the hybrid electrolyte. The Al corrosion and electrolyte decomposition side reactions at 5 V (*vs.* Li^+/Li) can be suppressed in 3 M LiTFSI 25%-IL electrolyte, in which good performance of a high-voltage $LiNi_{0.5}Mn_{1.5}O_4$ (LNMO) cathode is achieved. Capacities of 140 and 88 mA h g^{-1} were measured at 0.1 and 2C, respectively (*vs.* 25 mA h g^{-1} at 2C for a plain LiTFSI/PMP–TFSI IL electrolyte). After 300 charge–discharge cycles, 90% of the initial LNMO capacity was retained. This electrolyte also shows low flammability and great wettability toward a polyethylene separator. Moreover, this electrolyte allows elevated-temperature storage and operation of LNMO cells at 55 °C, which is not possible with the conventional carbonate electrolyte. Good compatibility of the electrolyte with a graphite anode is also demonstrated. The proposed electrolyte design concept has great potential for next-generation 5 V Li-ion batteries.

1. Introduction

Lithium-ion batteries (LIBs) are currently the dominant energy storage devices for portable electronics and electric vehicles.[1,2] Energy density and energy quality are both crucial.[3–5] High-voltage energy is more useful than low-voltage energy because of the square relationship between electrical power P and battery voltage V ($P = V^2/R$). Since the anode potential is limited to avoid Li metal electrodeposition, high-voltage cathodes are vital. Several high-voltage cathode candidates, such as nickel-rich layered oxides ($LiNi_{1-x}M_xO_2$, M = Co, Mn, and Al), lithium-rich layered oxides ($Li_{1+x}M_{1-x}O_2$, M = Mn, Ni, Co, *etc.*), spinel oxides (*e.g.*, $LiNi_{0.5}Mn_{1.5}O_4$), and polyanionic compounds (*e.g.*, phosphates, sulfates, and silicates), have been proposed.[6–8] However, the electrolyte is currently the bottleneck in the implementation of high-voltage LIBs.

The electrolyte greatly affects a battery's actual performance.[9,10] Unfortunately, a conventional carbonate electrolyte with $LiPF_6$ salt is unsuitable for high-voltage cathodes, especially at elevated temperature like 55 °C. The first problem is poor electrochemical stability of the carbonate solvent, which undergoes oxidative decomposition at >4.3 V (*vs.* Li^+/Li).[9,11] This solvent is also highly flammable, thermally unstable, and volatile.[12] High-voltage and high-temperature operations with this kind of electrolyte can lead to reliability and safety risks.[13] The second problem is associated with $LiPF_6$ salt, which can hydrolyze to generate LiF, POF_3, and HF.[14] In addition, $LiPF_6$ salt undergoes heterolytic dissociation at elevated temperature to form LiF precipitate and PF_5.[15–17] The reaction of PF_5 with residual water also produces HF, which tends to attack battery components.[15] The water content in the electrolyte can be lowered, which is costly and time-consuming, but it can never be completely eliminated, remaining at usually ~20 ppm.[14] The formation of HF is thus inevitable. Moreover, Li^+ is trapped in precipitated LiF, and this Li^+ loss degrades cell performance.[18] The use of an alternative Li salt, such as lithium bis(trifluoromethylsulfonyl)imide (LiTFSI), has thus attracted a lot of attention.[19–22] LiTFSI has superior electrochemical and thermal stability as well as lower sensitivity toward hydrolysis compared to those of $LiPF_6$.[23]

[a]Department of Materials Science and Engineering, National Chiao Tung University, 1001 University Road, Hsinchu 30010, Taiwan. E-mail: jkchang@nctu.edu.tw

[b]Department of Chemical and Materials Engineering, National Central University, Taoyuan, Taiwan

[c]Hierarchical Green-Energy Materials (Hi-GEM) Research Center, National Cheng Kung University, 1 University Road, Tainan, 701 Taiwan

[d]Department of Nuclear Science and Engineering, Department of Materials Science and Engineering, Massachusetts Institute of Technology, 77 Massachusetts Ave, Cambridge, MA 02139, USA. E-mail: liju@mit.edu

[e]Department of Energy Nanomaterials, Material & Chemical Research Laboratory, Industrial Technology Research Institute, Hsinchu 31040, Taiwan

† Electronic supplementary information (ESI) available. See DOI: 10.1039/c9ta04147h

Ionic liquid (IL) electrolytes (especially TFSI-based ILs), characterized by wide potential windows, excellent thermal and chemical stability, non-volatility, non-flammability, and environmental friendliness,[24–26] are potential candidates for high-voltage LIBs. However, the unsatisfactory high-rate performance of IL cells (traditionally ascribed to the low conductivity and high viscosity of ILs) and relatively high cost have limited practical applications. To overcome this problem, hybrid electrolytes that combine a TFSI-based IL with a carbonate solvent have attracted research interest. Appetecchi *et al.* investigated the physicochemical properties of a mixed electrolyte consisting of LiTFSI, *N*-propyl-*N*-methylpyrrolidinium (PMP)–TFSI IL, and ethylene carbonate (EC)/diethyl carbonate (DEC) co-solvent, and used this electrolyte with $Li_4Ti_5O_{12}$ and $LiFePO_4$ electrodes.[27] Balduci *et al.* showed that the addition of propylene carbonate into an LiTFSI/*N*-butyl-*N*-methylpyrrolidinium–TFSI IL electrolyte can reduce viscosity and improve $LiFePO_4$ charge–discharge performance.[28] Morita *et al.* significantly improved the electrochemical properties of both graphite and $LiMn_2O_4$ electrodes by introducing triethylphosphate and EC into an *N*-methyl-*N*-propylpiperidinium–TFSI IL electrolyte.[29] It is noted that this kind of hybrid electrolyte (TFSI-based IL/carbonate solvent) has been mainly used for low-voltage cathodes, such as $LiFePO_4$.[30–32] This could be ascribed to Al corrosion (LiTFSI was perceived to corrode Al in the presence of a carbonate solvent) and carbonate decomposition problems at high potential.[28,33,34] To the best of our knowledge, a TFSI-based IL/carbonate solvent hybrid electrolyte with LiTFSI salt has never been successfully applied to a high-voltage cathode.

In the present study, $LiNi_{0.5}Mn_{1.5}O_4$ (LNMO) is used as a model cathode because of its high charge–discharge potential of approximately 4.7 V (*vs.* Li^+/Li), unique three-dimensional ionic transport pathways, low cost, and environmental friendliness (it is cobalt-free).[35–37] Various ratios of PMP–TFSI IL and EC/DEC (1 : 1 by volume) solvent are systematically investigated. LiTFSI salt is used to avoid the drawbacks of $LiPF_6$. The LiTFSI concentration and IL ratio critically affect the electrolyte coordination states, which determine the irreversible side reaction (Al corrosion and carbonate decomposition) rate at high potential. The proposed electrolyte shows low flammability and great compatibility with both the LNMO cathode and graphite anode. This work proposes an electrolyte design strategy for high-safety and high-performance 5 V LIBs.

2. Experimental procedures

2.1 Preparation of LNMO powder and electrolytes

LNMO powder was synthesized using a co-precipitation method.[38] An aqueous solution of $NiSO_4 \cdot 6H_2O$ and $MnSO_4 \cdot H_2O$ was slowly pumped into a reactor at 50 °C. NH_4OH and NaOH solution was used to maintain the pH at 10.5. $Ni_{0.25}Mn_{0.75}(OH)_2$ precipitate with a particle diameter of 10–15 μm was thus obtained. This $Ni_{0.25}Mn_{0.75}(OH)_2$ was homogenously mixed with Li_2CO_3 powder and calcined at 750 °C in air for 12 h, producing LNMO powder.

PMP–TFSI IL, purchased from Solvionic (99.9%), was vacuum-dried at 100 °C for 24 h before use. An EC (Kishida, battery grade) and DEC (Kishida, battery grade) mixed solvent (1 : 1 by volume) was blended with PMP–TFSI IL and various concentrations of LiTFSI (99.8%, Sigma-Aldrich) to create hybrid electrolytes. A conventional electrolyte, consisting of EC/DEC (1 : 1 by volume) and 1 M $LiPF_6$ (Kishida, battery grade), was used for comparison. All the electrolytes were prepared in a glove box and dried using molecular sieves before use. The water content in the electrolytes, measured using a Karl Fisher titrator, was below 25 ppm. The ionic conductivity and viscosity of the electrolytes were measured using a TetraCon 325 conductivity meter and a Brookfield DV-I viscometer, respectively.

2.2 Cell assembly

The electrode slurry was prepared by mixing 80 wt% LNMO powder, 10 wt% super P, and 10 wt% poly(vinylidene fluoride) in *N*-methyl-2-pyrrolidone solution. The slurry was pasted onto Al foil and vacuum-dried at 100 °C for 12 h. The obtained electrode was then roll-pressed and punched to match the required dimensions of a CR2032 coin cell. Li foil and a glass fiber membrane were used as the counter electrode and the separator, respectively. The coin cells were assembled inside an argon-filled glove box (Innovation Technology Co. Ltd.), where both the moisture and oxygen content levels were maintained at below 0.3 ppm.

2.3 Material and electrochemical characterization

The LNMO powder was examined using scanning electron microscopy (SEM), X-ray diffraction (XRD), transmission electron microscopy (TEM), and Raman spectroscopy. Thermogravimetric analysis (TGA; Perkin-Elmer TGA7) was performed to evaluate the thermal stability of the electrolytes, which were heated from room temperature to 600 °C at a heating rate of 5 °C min^{-1} under a nitrogen atmosphere. The electrolyte flammability was tested under air according to a previously proposed method.[39] Briefly, a glass fiber membrane was used to adsorb electrolyte and then burned with an electric Bunsen burner. There was no air circulation and the distance between sample and fire was 123 mm. Linear sweep voltammetry (LSV) and electrochemical impedance spectroscopy (EIS) measurements were performed with a BiologicVSP-300 potentiostat. The charge–discharge properties (capacity, rate capability, and cycling stability) of the cells were evaluated using an Arbin BT-2043 battery tester. For each condition, at least five cells were measured. The performance deviation was typically within 5%, and the reported data are the median values.

3. Results and discussion

Fig. 1(a) shows the XRD pattern of our synthesized LNMO powder. All the diffraction peaks belong to a spinel crystal structure (JCPDS-80-2184) without any NiO or Li_xNi_yO impurity phases. The powder morphology examined using SEM is shown in Fig. 1(b), which reveals spherical aggregates that consist of rod-like substructures. The electron diffraction pattern in Fig. 1(c) shows an ordered array of diffraction spots that are

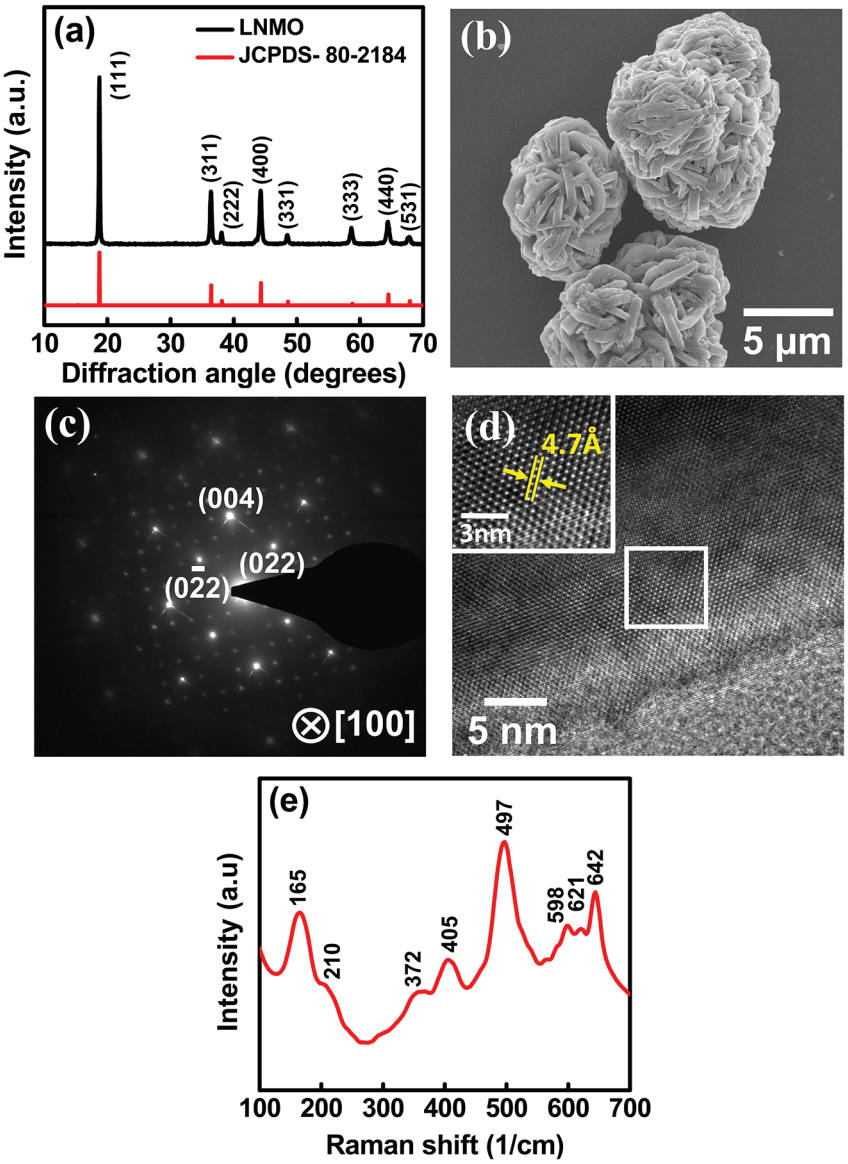

Fig. 1 (a) XRD pattern, (b) SEM image, (c) electron diffraction pattern, (d) high-resolution TEM image, and (e) Raman spectrum of synthesized LNMO powder.

associated with (022) and (004) planes of the cubic spinel structure. The appearance of extra diffraction spots with weaker intensity indicates the existence of Ni/Mn ordering in the crystal.[40,41] Fig. 1(d) shows a HRTEM micrograph, in which a highly ordered lattice of LNMO can be observed. The Raman spectrum in Fig. 1(e) exhibits distinguishable splitting of the F^1_{2g} band at 598 cm^{-1} and 621 cm^{-1}, which is characteristic of $P4_332$ space-group symmetry.[42,43] The clear peaks at 165 cm^{-1} and 210 cm^{-1} confirm that the Ni and Mn sites are well ordered in the LNMO lattice, indicative of a $P4_332$ (rather than $Fd\bar{3}m$) structure.[44]

The electrochemical stability windows of conventional 1 M $LiPF_6$/EC:DEC and 1 M LiTFSI/PMP–TFSI electrolytes are compared in Fig. 2(a). At a Pt electrode, the anodic decomposition potentials are ~4.2 and 5.6 V (*vs.* Li^+/Li), respectively. The high stability of TFSI anions against oxidation allows the wide potential stability window.[20,45] Fig. 2(b) shows the TGA data of the two electrolytes. The conventional carbonate electrolyte exhibits a significant weight loss of ~40% before 100 °C, where the solvent violently evaporates and $LiPF_6$ starts to decompose into LiF and PF_5.[12,46] At 200 °C, there was almost no residue left on the TGA crucible. In contrast, the decomposition temperature for the IL electrolyte is higher than 400 °C, indicating excellent thermal stability and low volatility. The flammability testing results in Fig. S1† reveal that the carbonate electrolyte ignited instantly and burned violently, whereas the IL electrolyte was not flammable and thus has fewer safety concerns. Fig. S2† shows the immersion test results of LNMO powder in the two electrolytes. Mn and Ni were clearly detected in the conventional electrolyte, whereas no dissolution of these elements was found in the IL electrolyte. The trace amounts of PF_5 and/or HF in the former electrolyte can attack LNMO,[47]

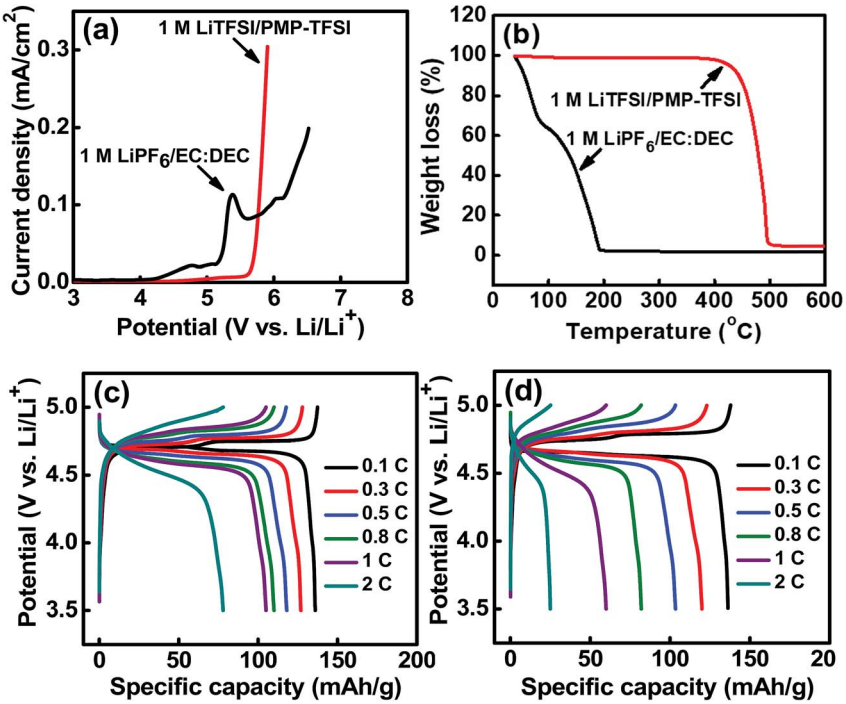

Fig. 2 (a) LSV scans of Pt electrodes recorded in 1 M $LiPF_6$/EC:DEC and 1 M LiTFSI/PMP–TFSI IL electrolytes with potential sweep rate of 1 mV s^{-1}. (b) TGA data for the two electrolytes. Charge–discharge curves of LNMO cells with 1 M LiTFSI/PMP–TFSI IL electrolyte recorded at various C rates at (c) 55 °C and (d) 25 °C.

leading to its dissolution. Fig. 2(c) shows the charge–discharge curves of the LNMO half cell with the IL electrolyte recorded at various C rates (1C ≡ 147 mA h g^{-1}) at 55 °C. Even at such elevated temperature and high cut-off potential of 5 V, great lithiation/delithiation performance was obtained. All the above properties indicate that the IL is an attractive LIB electrolyte.

The major hurdle of this electrolyte for practical applications is demonstrated in Fig. 2(d), which reveals the poor rate capability of the LNMO cell (with 1 M LiTFSI/PMP–TFSI IL electrolyte) at 25 °C. The measured capacity at 2C was as low as ~25 mA h g^{-1}, corresponding to only 18% retention compared to the capacity at 0.1C of 136 mA h g^{-1}. According to the literature,[9,48,49] this is associated with the inferior ionic conductivity and viscosity (1.2 mS cm^{-1} and 220 cP, respectively) of the 1 M LiTFSI/PMP–TFSI IL, in contrast to those (7.2 mS cm^{-1} and 3.7 cP, respectively) of the 1 M $LiPF_6$/EC:DEC electrolyte at 25 °C. In addition, the relatively low Li^+ transference number of the IL electrolyte is unfavorable for high-rate performance.[50,51] Improving the rate capability of high-voltage IL cells is our goal.

The organic carbonate solvent (EC:DEC = 1 : 1 by volume) was added into the IL electrolyte to modify its physiochemical properties. As shown in Fig. 3(a), with decreasing IL content (or increasing carbonate solvent ratio), the viscosity of the electrolyte monotonously decreases. For an LiTFSI concentration of 1 M, the optimal ionic conductivity of 6.6 mS cm^{-1} was found for the 25%-IL/75%-EC:DEC electrolyte. A further decrease in PMP–TFSI content reduced the total ion concentration in the electrolyte, resulting in lower conductivity. Unfortunately, none of these electrolytes (with various amounts of EC/DEC addition) allowed normal charge/discharge of the LNMO cells. Fig. 3(b) shows the representative charging curve for the 50%-IL cell. During charging, the electrode potential cannot reach the cut-off value, instead leveling off at ~4 V, which indicates the occurrence of some side reactions. Fig. 3(c) shows the linear sweep voltammetry (LSV) curves of bare Al foil in various electrolytes. In plain IL electrolyte, there was negligible current. The TFSI anions may either be inert (because few are in a free $TFSI^-$ state) or react with air-formed Al_2O_3 to generate the Al–TFSI complex, which is highly stable and insoluble in the IL electrolyte.[52] In addition, the adsorbed PMP anions on the electrode surface may also contribute to Al passivation.[53] With increasing carbonate solvent content, an irreversible anodic reaction, which took place at ~4 V, was promoted. The oxidation current is confirmed to be associated with Al pitting corrosion, as shown in Fig. 3(d). In the presence of carbonate solvent, probably due to its high dielectric constant, soluble $[Al(TFSI)_x]^{(3-x)+}$ species are generated,[54] leading to the dissolution of Al. We believe that this has prevented any successful use of this hybrid electrolyte for high-voltage cathodes in the literature.

Of note, we found that the LiTFSI concentration significantly affects the LSV current. As shown in Fig. 4(a) and (b), higher LiTFSI concentrations (*i.e.*, 2 M and 3 M) lead to lower anodic current densities at high potential compared to those in Fig. 3(c) (*i.e.*, 1 M). The SEM images in Fig. 4(c) and (d) confirm that Al corrosion is indeed suppressed by increasing the concentration of LiTFSI. Raman spectroscopic analyses were conducted to gain insight into the coordination structures of the electrolytes. As shown in Fig. 5, various vibrational modes of

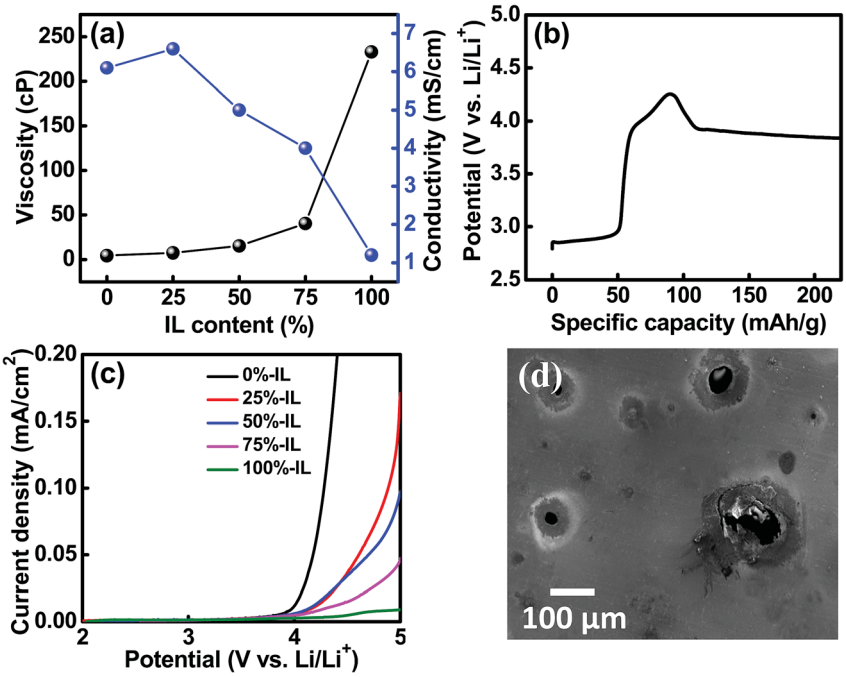

Fig. 3 (a) Viscosity and conductivity values of IL/EC:DEC mixed electrolytes with 1 M LiTFSI. (b) Charging curve of 1 M LiTFSI/50%-IL LNMO cell. (c) LSV curves of Al electrodes recorded in various electrolytes with 1 M LiTFSI. (d) SEM image of Al electrode after LSV test in 1 M LiTFSI/50%-IL electrolyte.

$TFSI^-$ are found in the range of 720–780 cm^{-1}, depending on the coordination state. The band at ~740 cm^{-1} is assigned to free $TFSI^-$ anions (*i.e.*, in a solvent-separated state) without direct interaction with cations.[55] When a $TFSI^-$ anion is coordinated with one or more cations, forming a contact ion pair (CIP) or an aggregate (AGG), the band shifts to ~745 or ~750 cm^{-1}.[52] As shown in the figure, the 1 M 50%-IL electrolyte has a dominant amount of free $TFSI^-$, which favorably associate with Al to form soluble $[Al(TFSI)_x]^{(3-x)+}$ species in the hybrid electrolyte,[56] leading to Al dissolution. With increasing LiTFSI

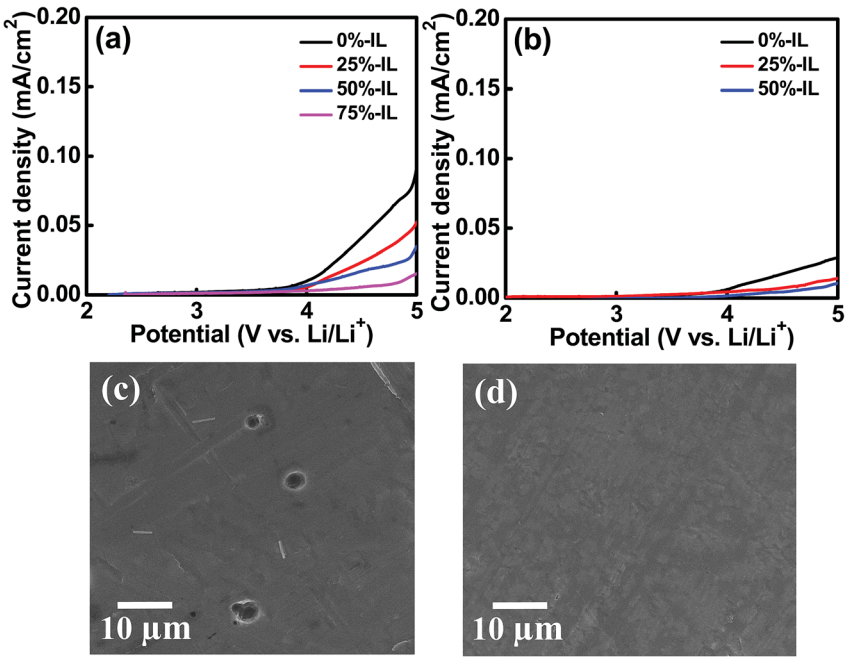

Fig. 4 LSV curves of Al electrodes recorded in various electrolytes with (a) 2 M and (b) 3 M LiTFSI. SEM images of Al electrodes after LSV tests in (c) 2 M LiTFSI/50%-IL and (d) 3 M LiTFSI/25%-IL electrolytes.

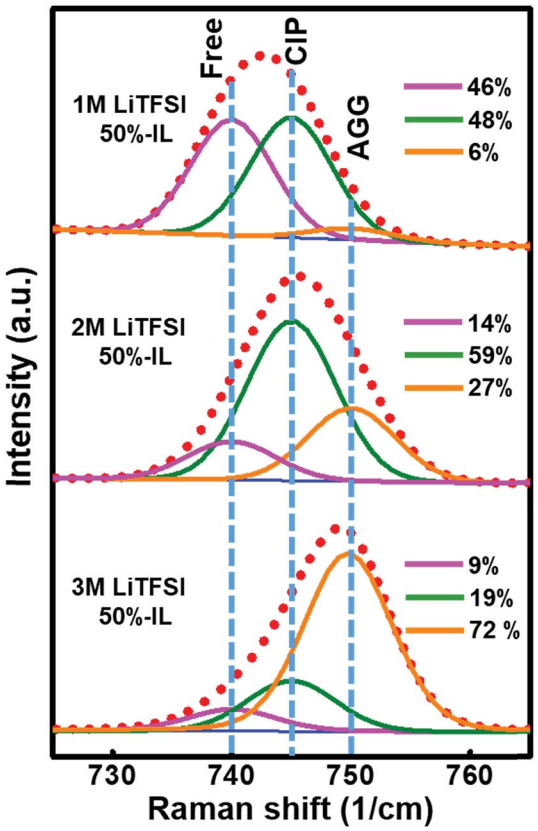

Fig. 5 Raman spectra of 50%-IL electrolytes with various concentrations of LiTFSI.

concentration, the free $TFSI^-$ signal decreases, whereas the CIP and AGG components increase. In 3 M 50%-IL electrolyte, most of the $TFSI^-$ anions coordinate with electrolyte cations and thus have less activity toward reaction with Al.[55,56] It is also noted that Li^+ at a high concentration can solvate (or "fix") a large amount of carbonate solvent molecules (with a high dielectric constant),[55,57] constraining the solubility of $[Al(TFSI)_x]^{(3-x)+}$ in the electrolyte.

Fig. S3† shows the chronoamperometry data of Al electrodes recorded in various electrolytes at 5 V. The measured anodic current can be attributed to the anodic dissolution of Al and electrolyte decomposition. The data indicate that these side reactions are progressively inhibited with increasing LiTFSI and IL content. As shown in the Raman spectra in Fig. S4,† increasing the IL ratio favors the formation of CIP and AGG states, which decrease corrosivity. The IL also plays another role. The carbonate solvent molecules can partially donate their electrons to Li^+ and PMP^+ cations[58–60] and thus extend their anodic potential limit (because the release of another electron becomes more difficult). This argument is supported by Fig. S5,† in which 3 M 25%-IL electrolyte shows a higher decomposition potential than that of 3 M 0%-IL electrolyte. These data suggest that the LiTFSI, IL, and carbonate solvent ratio in the electrolyte should be properly designed to meet the requirements for high-voltage battery applications.

Table 1 Side reaction current densities (μA cm^{-2}) of Al electrodes after being held at 5 V for 12 hours in various electrolytes[a]

	EC:DEC	25% IL	50% IL	75% IL	100% IL
1 M	28 372.5	2288.1	1051.1	373.1	0.4
2 M	761.9	485.5	159.8	5.5	—
3 M	122.1	1.2	1.1	—	—

[a] —: excess of solubility.

Table 1 summarizes the side reaction current densities of the Al electrodes after 12 h shown in Fig. S3.† Interestingly, we found that as long as the side-reaction current density listed in Table 1 is higher than 10 μA cm^{-2}, the correspondingly assembled LNMO cells cannot normally function (the charging curves are similar to that in Fig. 3(b)). For example, the charging curves of the 3 M LiTFSI/0%-IL cell is shown in Fig. S6.† Fig. S7† compares the cyclic voltammetry of the 3 M LiTFSI/0%-IL and 3 M LiTFSI/25%-IL cells. The former cell showed a clear irreversible anodic reaction at high voltage, whereas the latter cell exhibited ideal reversible Ni^{2+}/N^{3+} and Ni^{3+}/Ni^{4+} transitions between 4.6–4.9 V. Fig. 6(a)–(c) show the charge–discharge performance of the cells with 2 M LiTFSI/75%-IL, 3 M LiTFSI/25%-IL, and 3 M LiTFSI/50%-IL electrolytes (whose side reaction current densities are lower than 10 μA cm^{-2}), respectively, at 25 °C. The capacities measured at 0.1C for all cells are ~140 mA h g^{-1}. However, the capacity retention ratios at 2C are 46%, 63%, and 15%, respectively, in contrast to 18% for the plain IL cell (Fig. 2(d)), indicating that the rate capability can be greatly improved if an optimized electrolyte is used. The ionic conductivity (viscosity) values of 2 M LiTFSI/75%-IL, 3 M LiTFSI/25%-IL, 3 M LiTFSI/50%-IL, and 1 M LiTFSI/100%-IL electrolytes are 0.5, 0.7, 0.3, and 1.2 mS cm^{-1}, respectively (294, 255, 369, and 220 cP, respectively). Clearly, the electrolyte conductivity and viscosity are not the determining factors of cell rate capability. The hybrid electrolytes, even with lower conductivity and higher viscosity, enable better high-rate performance than that for the plain IL electrolyte.

EIS was used to further examine the impedance characteristics of various cells; the obtained data are shown in Fig. 6(d). The Nyquist spectra are composed of a semicircle at high frequency and a sloping line at low frequency, which can be characterized by the equivalent circuit shown in the figure inset, where R_e, R_{ct}, CPE, and W are the electrolyte resistance, interfacial charge transfer resistance, interfacial constant phase element, and Warburg impedance associated with Li^+ diffusion inside the electrode active material, respectively.[61] The R_{ct} values, which are related to the Nyquist semicircle diameters, are 530, 400, 960, and 830 Ω, respectively, for the 2 M LiTFSI/75%-IL, 3 M LiTFSI/25%-IL, 3 M LiTFSI/50%-IL, and 1 M LiTFSI/100%-IL cells. R_{ct}, not R_e, thus mainly governs the cell high-rate capability. A high Li^+ concentration with sufficient carbonate solvent content seems to facilitate Li^+ desolvation (or decoupling from CIPs/AGGs) reactions, decreasing the charge transfer resistance. The composition of the cathode/electrolyte interface film also crucially affects the R_{ct} magnitude. Further material

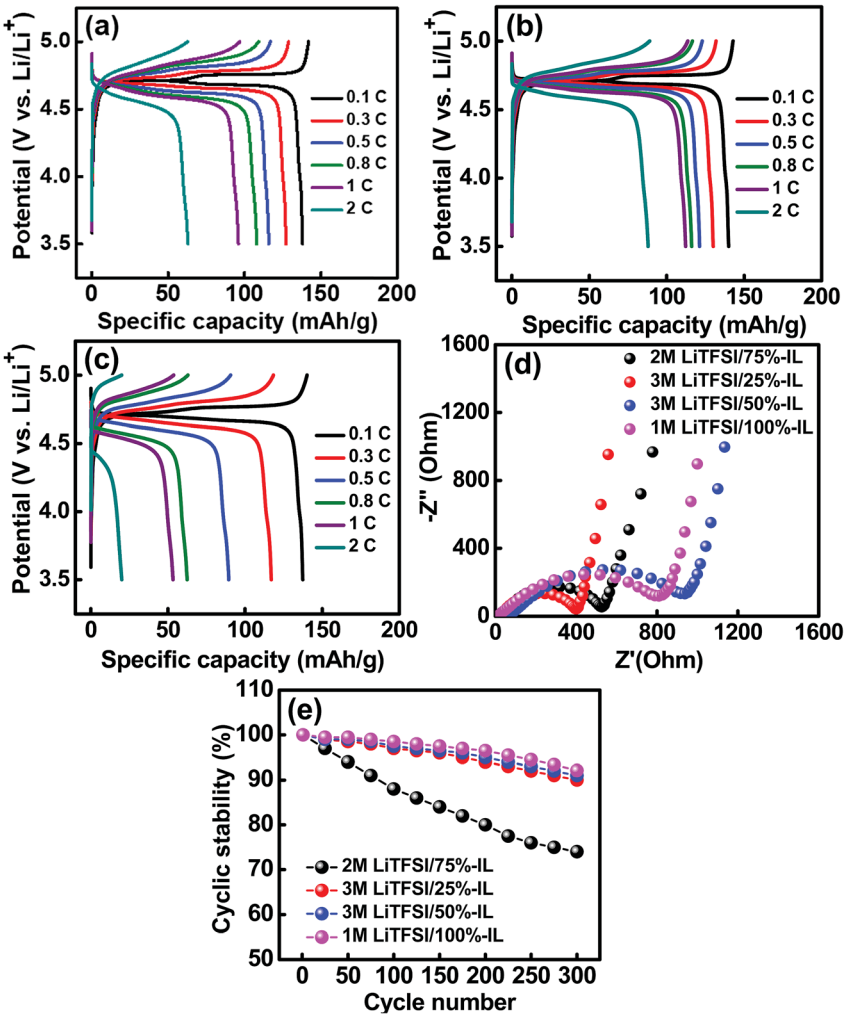

Fig. 6 Charge–discharge curves of cells with (a) 2 M LiTFSI/75%-IL, (b) 3 M LiTFSI/25%-IL, and (c) 3 M LiTFSI/50%-IL electrolytes recorded at 25 °C. (d) EIS and (e) cyclic stability data of LNMO cells with various electrolytes.

and electrochemical investigations are required to clarify the interface properties.

Fig. 6(e) compares the cycling stability of LNMO cells with various electrolytes measured at 1C. After 300 charge–discharge cycles, the 2 M LiTFSI/75%-IL, 3 M LiTFSI/25%-IL, 3 M LiTFSI/50%-IL, and 1 M LiTFSI/100%-IL cells retained 74%, 90%, 91%, and 92% of their initial capacities, respectively. This trend is in line with the side-reaction current densities listed in Table 1. Less Al corrosion and electrolyte decomposition are essential for the long cycle life of batteries. It is noted that the conventional carbonate electrolyte (1 M $LiPF_6$/EC:DEC) cell showed 20% capacity decay after the same number of cycles. The results show that the 3 M LiTFSI/25%-IL electrolyte not only leads to superior LNMO rate capability but also ensures satisfactory cell durability. Fig. S8† shows the electrolyte Raman data before and after 20 charge–discharge cycles. The consistent spectra suggest that the coordination status of the 3 M LiTFSI/25%-IL electrolyte is stable upon cycling.

Fig. 7(a) shows the low flammability of the 3 M LiTFSI/25%-IL electrolyte. Due to the high LiTFSI concentration and IL incorporation, most of the carbonate molecules are solvated, leaving less free solvent to evaporate and cause fire.[62] Thus, this electrolyte is much safer than the conventional carbonate electrolyte (see Fig. S1†). Although the plain IL electrolyte has difficulty penetrating commercial separators.[63] Fig. 7(b) reveals that the 3 M LiTFSI/25%-IL electrolyte can readily wet a polyethylene separator. Fig. 7(c) shows the great charge–discharge properties of the 3 M LiTFSI/25%-IL cell recorded at 55 °C after being stored at the same temperature for one week. Because Li^+ mobility in both the electrolyte and electrode was enhanced, excellent lithiation/delithiation kinetics was observed. At a rate of 2C, a decent capacity of 95 mA h g^{-1} was obtained. In contrast, the conventional electrolyte (1 M $LiPF_6$/EC:DEC) cell failed under the same testing protocol (data are shown in Fig. S9†). Under such harsh conditions, the carbonate electrolyte is thermally and electrochemically unstable, leading to cell failure. To verify the compatibility of the proposed electrolyte with the LIB anode, a graphite/Li half cell was examined. As shown in Fig. 7(d), good charge–discharge performance with great rate capability was found, in sharp contrast to the poor

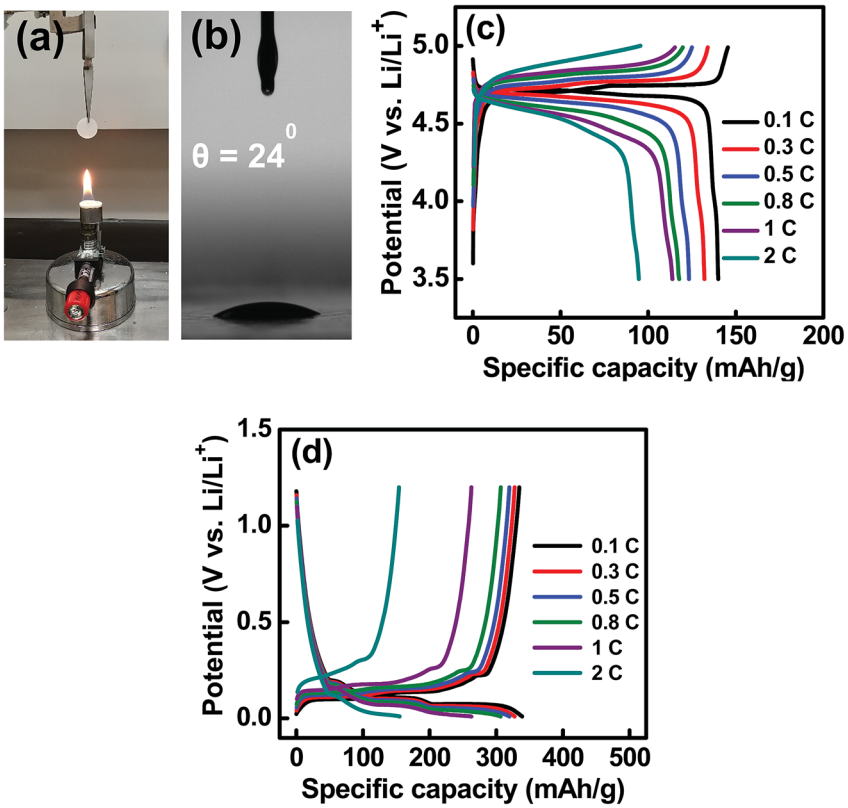

Fig. 7 (a) Flammability and (b) wettability toward a polyethylene separator of 3 M LiTFSI/25%-IL electrolyte. (c) Charge–discharge curves of LNMO cell with 3 M LiTFSI/25%-IL recorded at 55 °C after being stored at the same temperature for one week. (d) Charge–discharge performance of graphite electrode in 3 M LiTFSI/25%-IL electrolyte.

compatibility between the plain TFSI-based IL electrolyte and graphite anodes.[64–66] It is believed that the incorporated EC and high-concentration LiTFSI help generate an effective solid-electrolyte interphase layer on the graphite surface, enabling the highly reversible Li^+ intercalation/deintercalation reactions. The proposed electrolyte is highly promising for high-safety and high-reliability 5 V LIB applications.

4. Conclusions

This study showed that the Al corrosion problem of TFSI-based IL/carbonate solvent hybrid electrolytes can be effectively suppressed by simply adjusting the LiTFSI concentration (without the use of $LiPF_6$ or sophisticated salts and additives) in the electrolyte. The IL to carbonate solvent ratio crucially affects the coordination states in the electrolyte, which influence corrosivity toward Al. A high Li^+ concentration and the co-existence of the IL extend the anodic decomposition potential of the carbonate solvent, reducing the side reactions up to 5 V. The rate capability of the LNMO cell was considerably improved by using the proposed electrolyte, as compared to using a plain 1 M LiTFSI/PMP–TFSI IL electrolyte. R_{ct}, not R_e, was confirmed to be the determining factor of cell high-rate performance. The 3 M LiTFSI 25%-IL electrolyte is cost-effective (consisting of 75% conventional carbonate solvent), non-flammable, and highly reliable (allowing great cycling stability and 55 °C operation of the LNMO cell). In addition, good wettability toward a polyethylene separator and great compatibility with a graphite anode were demonstrated for this electrolyte. This work proposed a feasible strategy that involves modulating the Li salt concentration and IL/carbonate ratio for developing hybrid electrolytes for 5 V LIB applications.

Conflicts of interest

The authors declare no competing financial interests.

Acknowledgements

The financial support provided for this work by the Ministry of Science and Technology (MOST) of Taiwan is gratefully appreciated (grant no. 107-2811-E-009-530 and 107-2923-E-007-001). JL acknowledges support by NSF ECCS-1610806.

References

1 C. Liu, F. Li, L. Ma and H. M. Cheng, *Adv. Mater.*, 2010, **22**, E28.
2 W. Li, B. Song and A. Manthiram, *Chem. Soc. Rev.*, 2017, **46**, 3006.
3 M. S. Whittingham, *Chem. Rev.*, 2004, **104**, 4271.

4 W. Weppner and R. A. Huggins, *J. Electrochem. Soc.*, 1978, **125**, 7.
5 J. L. Shi, D. D. Xiao, M. Ge, X. Yu, Y. Chu, X. Huang, X. D. Zhang, Y. X. Yin, X. Q. Yang, Y. G. Guo, L. Gu and L. J. Wan, *Adv. Mater.*, 2018, **30**, 1705575.
6 M. Hu, X. Pang and Z. Zhou, *J. Power Sources*, 2013, **237**, 229.
7 B. Li and D. Xia, *Adv. Mater.*, 2017, **29**, 1701054.
8 A. Manthiram, J. C. Knight, S. T. Myung, S. M. Oh and Y. K. Sun, *Adv. Energy Mater.*, 2016, **6**, 1501010.
9 K. Xu, *Chem. Rev.*, 2014, **114**, 11503.
10 J. Kalhoff, G. G. Eshetu, D. Bresser and S. Passerini, *ChemSusChem*, 2015, **8**, 2154.
11 L. Xing, W. Li, C. Wang, F. Gu, M. Xu, C. Tan and J. Yi, *J. Phys. Chem. B*, 2009, **113**, 16596.
12 T. Kawamura, S. Okada and J. I. Yamaki, *J. Power Sources*, 2006, **156**, 547.
13 R. Wagner, M. Korth, B. Streipert, J. Kasnatscheew, D. R. Gallus, S. Brox, M. Amereller, I. C. Laskovic and M. Winter, *ACS Appl. Mater. Interfaces*, 2016, **8**, 30871.
14 J. B. Goodenough and Y. Kim, *Chem. Mater.*, 2010, **22**, 587.
15 J. L. Tebbe, T. F. Fuerst and C. B. Musgrave, *J. Power Sources*, 2015, **297**, 427.
16 D. Aurbach, B. Markovsky, G. Salitra, E. Markevich, Y. Talyossef, M. Koltypin, L. Nazar, B. Ellis and D. Kovacheva, *J. Power Sources*, 2007, **165**, 491.
17 H. Yang, G. V. Zhuang and P. N. Ross Jr, *J. Power Sources*, 2006, **161**, 573.
18 J. L. Tebbe, A. M. Holder and C. B. Musgrave, *ACS Appl. Mater. Interfaces*, 2015, **7**, 24265.
19 T. Vogl, S. Menne, R. S. Kuhnel and A. Balducci, *J. Mater. Chem. A*, 2014, **2**, 8258.
20 P. Meister, X. Qi, R. Kloepsch, E. Kramer, B. Streipert, M. Winter and T. Placke, *ChemSusChem*, 2017, **10**, 804.
21 D. W. McOwen, D. M. Seo, O. Borodin, J. Vatamanu, P. D. Boyle and W. A. Henderson, *Energy Environ. Sci.*, 2014, **7**, 416.
22 H. Zhang, W. Qu, N. Chen, Y. Huang, L. Li, F. Wu and R. Chen, *Electrochim. Acta*, 2018, **285**, 78.
23 K. Matsumoto, K. Inoue, K. Nakahara, R. Yuge, T. Noguchi and K. Utsugi, *J. Power Sources*, 2013, **231**, 234.
24 M. Watanabe, M. L. Thomas, S. Zhang, K. Ueno, T. Yasuda and K. Dokko, *Chem. Rev.*, 2017, **117**, 7190.
25 M. Armand, F. Endres, D. R. MacFarlane, H. Ohno and B. Scrosati, *Nat. Mater.*, 2009, **8**, 621.
26 D. R. MacFarlane, N. Tachikawa, M. Forsyth, J. M. Pringle, P. C. Howlett, G. D. Elliott, J. H. Davis, M. Watanabe, P. Simon and C. A. Angell, *Energy Environ. Sci.*, 2014, **7**, 232.
27 M. Montanino, M. Moreno, M. Carewska, G. Maresca, E. Simonetti, R. Lo Presti, F. Alessandrini and G. B. Appetecchi, *J. Power Sources*, 2014, **269**, 608.
28 R. S. Kuhnel, N. Böckenfeld, S. Passerini, M. Winter and A. Balducci, *Electrochim. Acta*, 2011, **56**, 4092.
29 B. S. Lalia, N. Yoshimoto, M. Egashira and M. Morita, *J. Power Sources*, 2010, **195**, 7426.
30 I. Quinzeni, S. Ferrari, E. Quartarone, C. Tomasi, M. Fagnoni and P. Mustarelli, *J. Power Sources*, 2013, **237**, 204.
31 T. Vogl, S. Menne and A. Balducci, *Phys. Chem. Chem. Phys.*, 2014, **16**, 25014.
32 B. Yang, C. Li, J. Zhou, J. Liu and Q. Zhang, *Electrochim. Acta*, 2014, **148**, 39.
33 W. K. Behl and E. J. Plichta, *J. Power Sources*, 1998, **72**, 132.
34 E. Cho, J. Mun, O. B. Chae, O. M. Kwon, H. T. Kim, J. H. Ryu, Y. G. Kim and S. M. Oh, *Electrochem. Commun.*, 2012, **22**, 1.
35 A. Manthiram, K. Chemelewski and E. S. Lee, *Energy Environ. Sci.*, 2014, **7**, 1339.
36 B. Chen, L. Ben, Y. Chen, H. Yu, H. Zhang, W. Zhao and X. Huang, *Chem. Mater.*, 2018, **30**, 2174.
37 J. Chong, S. Xun, X. Song, G. Liu and V. Battaglia, *Nano Energy*, 2013, **2**, 283.
38 W. K. Pang, H. F. Lin, V. K. Peterson, C. Z. Lu, C. E. Liu, S. C. Liao and J. M. Chen, *J. Phys. Chem. C*, 2017, **121**, 3680.
39 C. Arbizzani, G. Gabrielli and M. Mastragostino, *J. Power Sources*, 2011, **196**, 4801.
40 J. H. Kim, A. Huq, M. Chi, N. P. W. Pieczonka, E. Lee, C. A. Bridges, M. M. Tessema, A. Manthiram, K. A. Persson and B. R. Powell, *Chem. Mater.*, 2014, **26**, 4377.
41 J. H. Kim, S. T. Myung, C. S. Yoon, S. G. Kang and Y. K. Sun, *Chem. Mater.*, 2004, **16**, 906.
42 A. K. Haridas, C. S. Sharma and T. N. Rao, *Electrochim. Acta*, 2016, **212**, 500.
43 J. Yang, X. Han, X. Zhang, F. Cheng and J. Chen, *Nano Res.*, 2013, **6**, 679.
44 J. Wang, W. Lin, B. Wu and J. Zhao, *J. Mater. Chem. A*, 2014, **2**, 16434.
45 S. Kazemiabnavi, Z. Zhang, K. Thornton and S. Banerjee, *J. Phys. Chem. B*, 2016, **120**, 5691.
46 K. Xu, *Chem. Rev.*, 2004, **104**, 4303.
47 N. P. W. Pieczonka, Z. Liu, P. Lu, K. L. Olson, J. Moote, B. R. Powell and J. H. Kim, *J. Phys. Chem. C*, 2013, **117**, 15947.
48 Y. S. Fung, Y. Yang, J. Zheng and D. Zhu, *ECS Trans.*, 2012, **50**, 57.
49 H. F. Xiang, B. Yin, H. Wang, H. W. Lin, X. W. Ge, S. Xie and C. H. Chen, *Electrochim. Acta*, 2010, **55**, 5204.
50 N. Wongittharom, C. H. Wang, Y. C. Wang, G. T. K. Fey, H. Y. Li, T. Y. Wu, T. C. Lee and J. K. Chang, *J. Power Sources*, 2014, **260**, 268.
51 K. Oldiges, D. Diddens, M. Ebrahiminia, J. B. Hooper, I. Cekic-Laskovic, A. Heuer, D. Bedrov, M. Winter and G. Brunklaus, *Phys. Chem. Chem. Phys.*, 2018, **20**, 16579.
52 I. A. Shkrob, K. Z. Pupek and D. P. Abraham, *J. Phys. Chem. C*, 2016, **120**, 18435.
53 S. Theivaprakasam, G. Girard, P. Howlett, M. Forsyth, S. Mitra and D. MacFarlane, *npj Mater. Degrad.*, 2018, **2**, 13.
54 R. S. Kuhnel, M. Lubke, M. Winter, S. Passerini and A. Balducci, *J. Power Sources*, 2012, **214**, 178.
55 Y. Yamada, K. Furukawa, K. Sodeyama, K. Kikuchi, M. Yaegashi, Y. Tateyama and A. Yamada, *J. Am. Chem. Soc.*, 2014, **136**, 5039.
56 D. W. McOwen, D. M. Seo, O. Boorodin, J. Vatamanu, P. D. Boyle and W. A. Henderson, *Energy Environ. Sci.*, 2014, **7**, 416.
57 Y. Yamada and A. Yamada, *J. Electrochem. Soc.*, 2015, **162**, A2406.

58 Y. Yamada and A. Yamada, *Chem. Lett.*, 2017, **46**, 1056.
59 Y. Yamada, *Electrochemistry*, 2017, **85**, 559.
60 K. Sodeyama, Y. Yamada, K. Aikawa, A. Yamada and Y. Tateyama, *J. Phys. Chem. C*, 2014, **118**, 14091.
61 J. Patra, H. T. Huang, W. Xue, C. Wang, A. S. Helal, J. Li and J. K. Chang, *Energy Storage Materials*, 2019, **16**, 146.
62 S. Wilken, S. Xiong, J. Scheers, P. Jacobsson and P. Johansson, *J. Power Sources*, 2015, **275**, 935.
63 C. S. Stefan, D. Lemordant, B. C. Montigny and D. Violleau, *J. Power Sources*, 2009, **189**, 1174.
64 H. Zheng, K. Jiang, T. Abe and Z. Ogumi, *Carbon*, 2006, **44**, 203.
65 S. Seki, Y. Kobayashi, H. Miyashiro, Y. Ohno, Y. Mita and N. Terada, *J. Phys. Chem. C*, 2008, **112**, 16708.
66 S. Rothermel, P. Meister, O. Fromm, J. Huesker, H. W. Meyer, M. Winter and T. Placke, *ECS Trans.*, 2014, **58**, 15.

Electronic Supplementary Information for

Hybrid electrolyte enables safe and practical 5-V $LiNi_{0.5}Mn_{1.5}O_4$ batteries

Purna Chandra Rath, Chia-Jung Wu, Jagabandhu Patra, Ju Li*, Tai-Chou Lee,

Ting-Ju Yeh, Jeng-Kuei Chang*

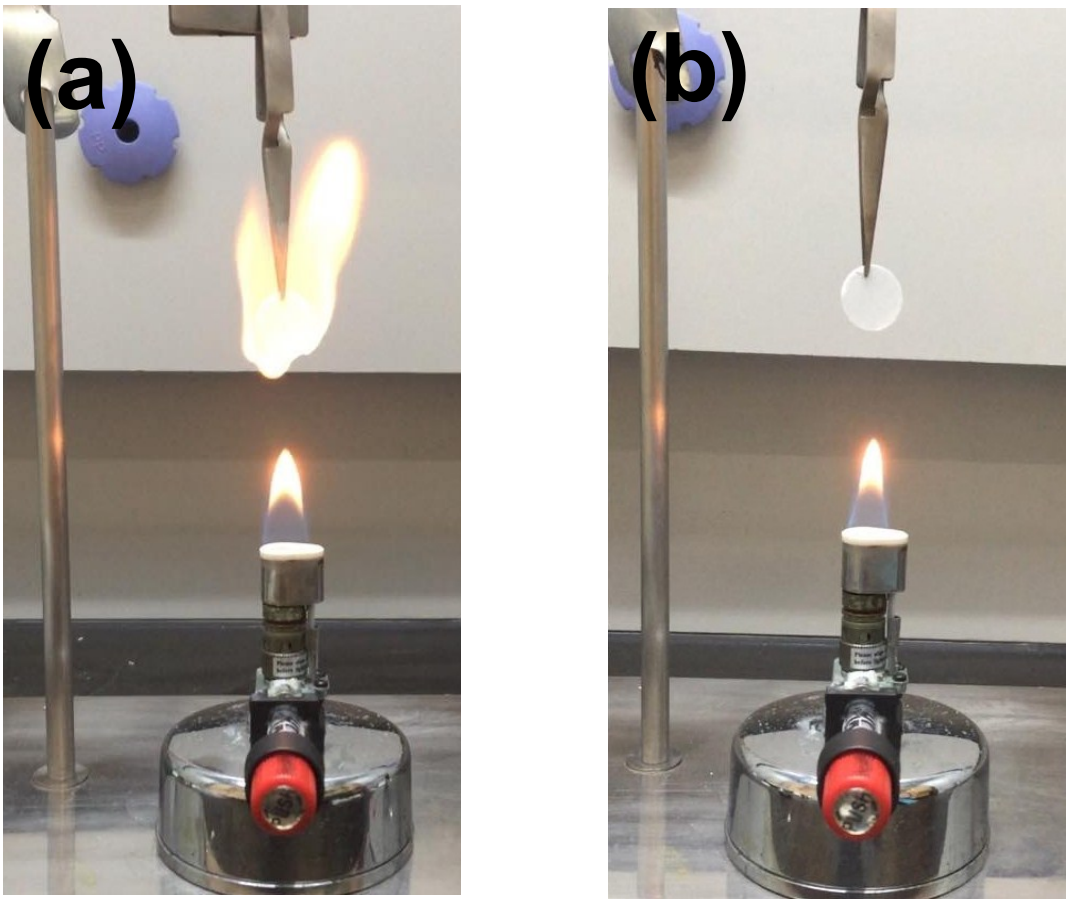

Figure S1. Flammability testing results of (a) 1 M $LiPF_6$/EC:DEC and (b) 1 M LiTFSI/PMP–TFSI IL electrolytes.

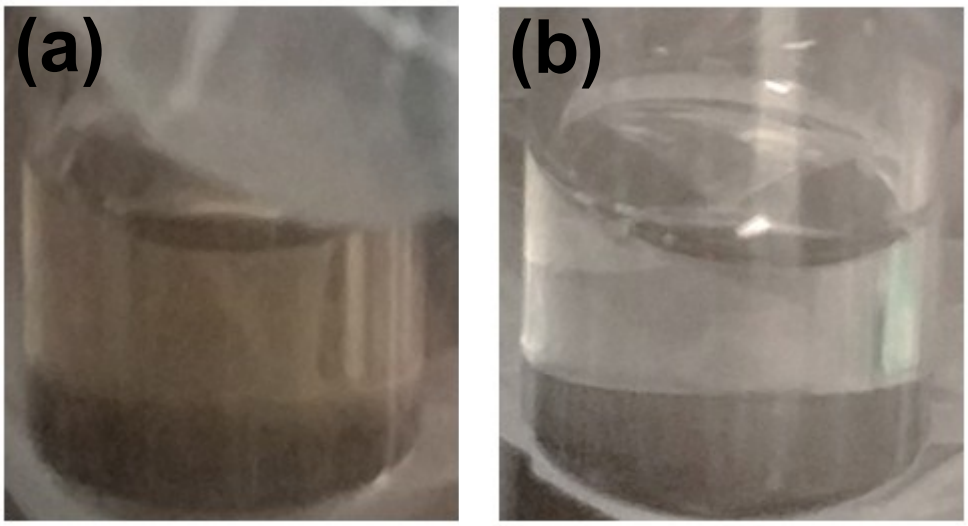

(c) Electrolyte	Mn concentration	Ni concentration
1 M $LiPF_6$/EC:DEC	514 ppm	103 ppm
1 M LiTFSI/PMP–TFSI	Not detectable	Not detectable

Figure S2. Immersion tests of LNMO powder (0.5 g) in 2 mL of (a) 1 M $LiPF_6$/EC:DEC and (b) 1 M LiTFSI/PMP–TFSI IL electrolytes after 1 month. (c) Concentrations of Mn and Ni dissolved in the electrolytes.

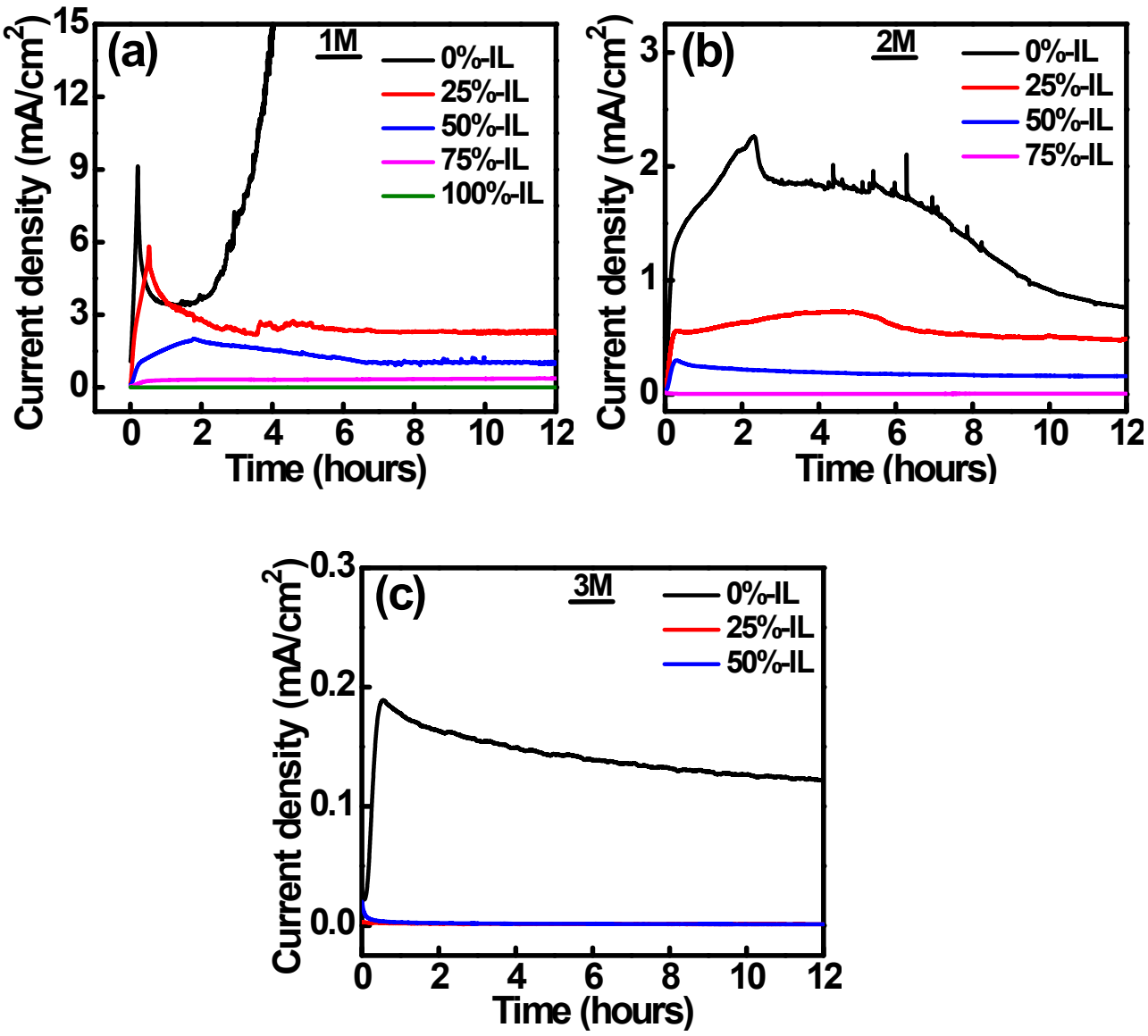

Figure S3. Chronoamperometry data of Al electrodes recorded in various electrolytes with (a) 1 M, (b) 2 M, and (c) 3 M LiTFSI at 5 V.

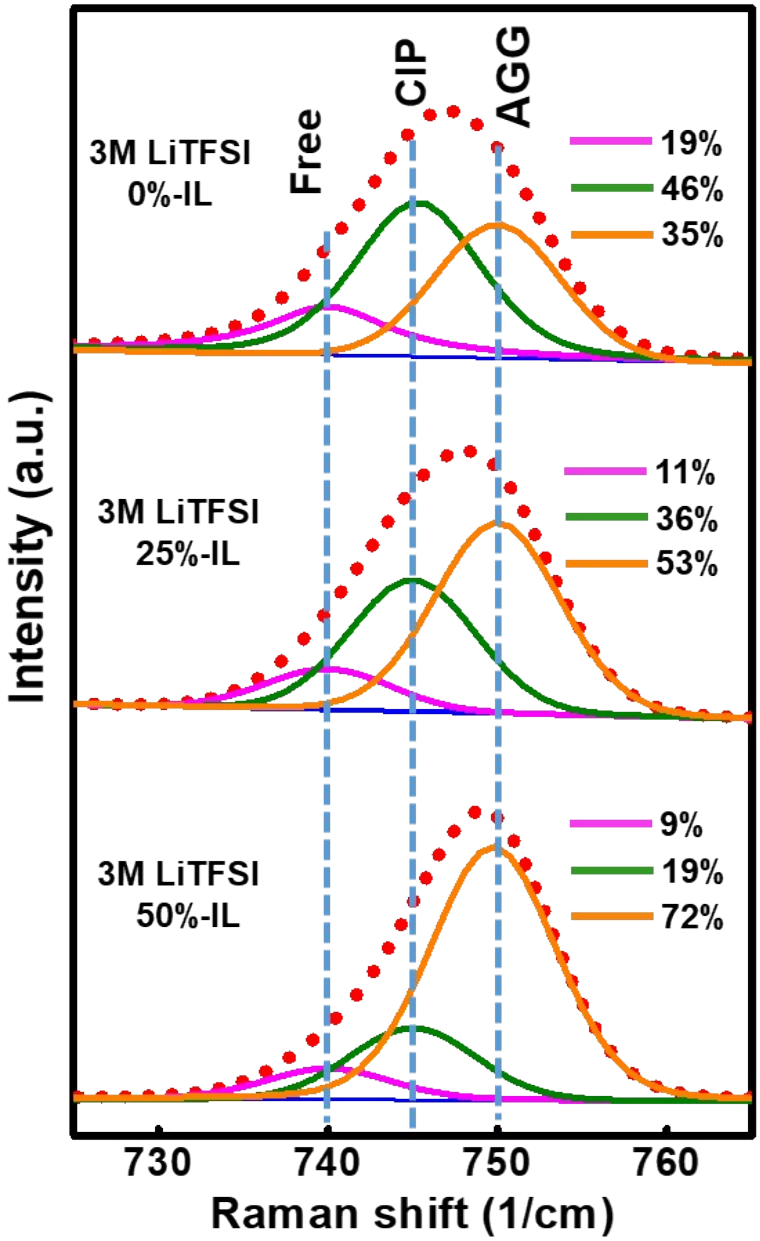

Figure S4. Raman spectra of 3 M LiTFSI/0%-IL, 3 M LiTFSI/25%-IL, and 3 M LiTFSI/50%-IL electrolytes.

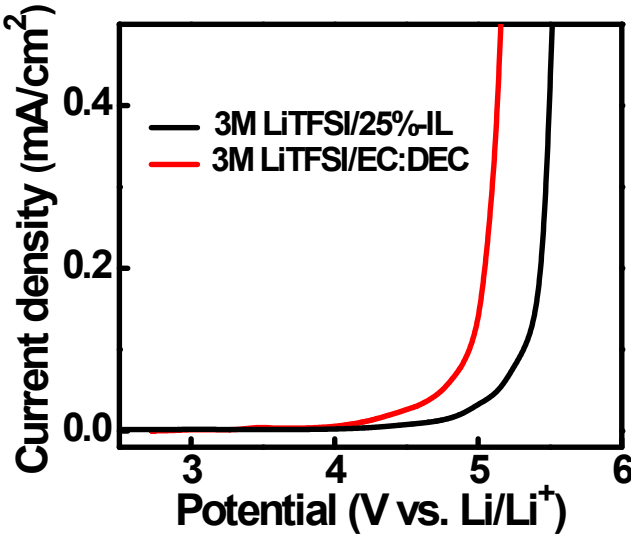

Figure S5. LSV curves of Pt electrodes recorded in 3 M LiTFSI/0%-IL and 3 M LiTFSI/25%-IL electrolytes with potential sweep rate of 1 mV s^{-1}.

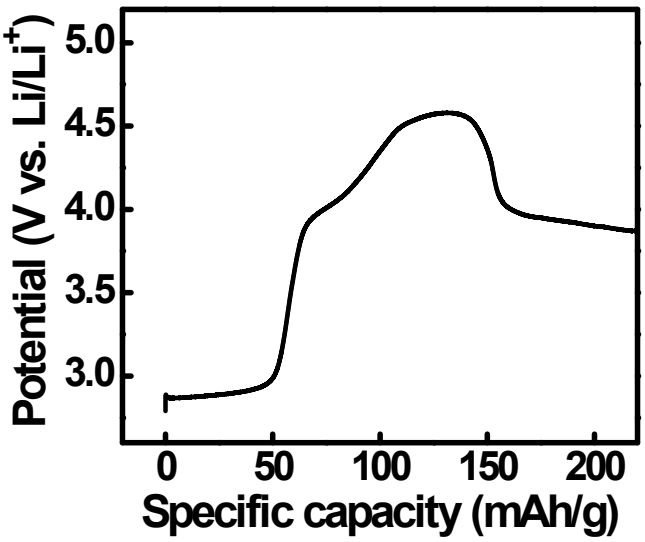

Figure S6. Charging curve of 3 M LiTFSI/0%-IL LNMO cell

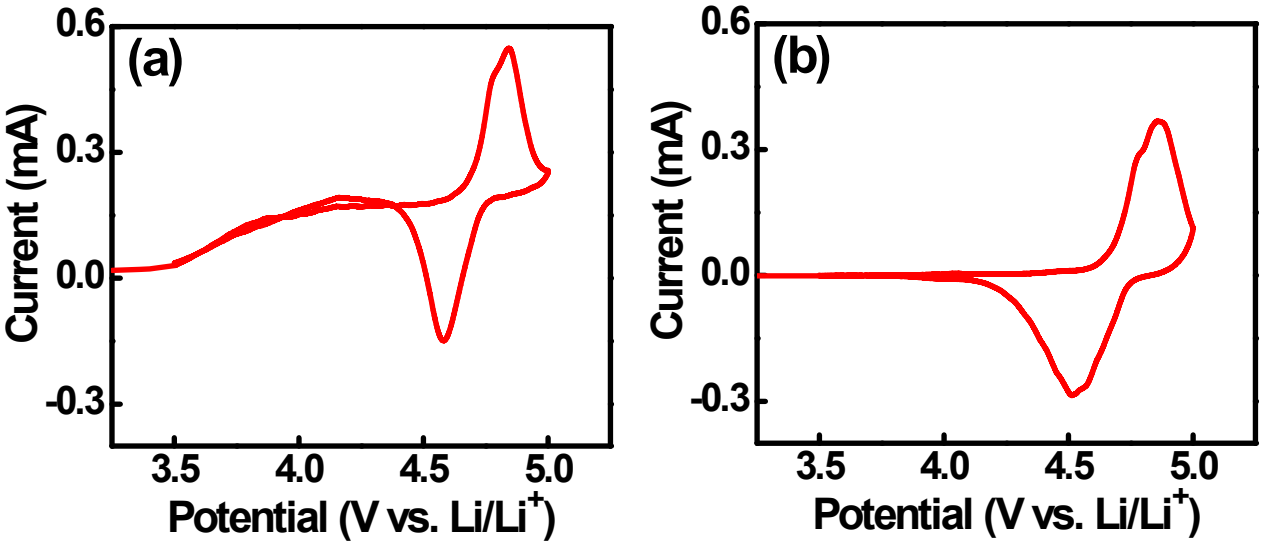

Figure S7. Cyclic voltammetry data of LNMO cells with (a) 3 M LiTFSI/0%-IL and (b) 3 M LiTFSI/25%-IL electrolytes recorded at 0.1 mV s^{-1}.

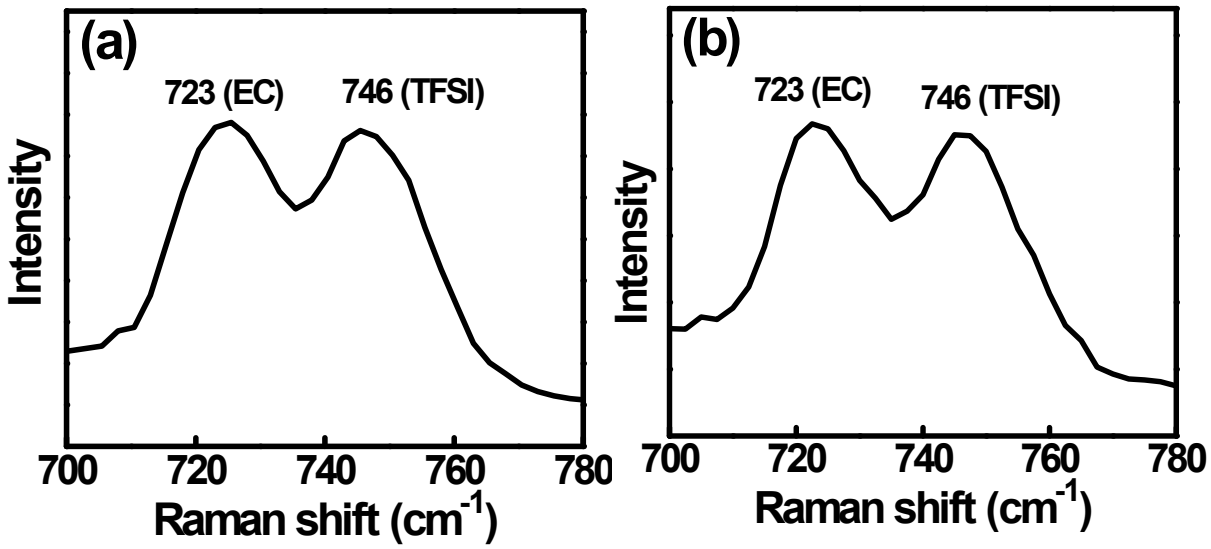

Figure S8. Raman spectra of (a) fresh 3 M LiTFSI/25%-IL electrolyte and (b) the same electrolyte after 20 charge-discharge cycles extracted from LNMO cell.

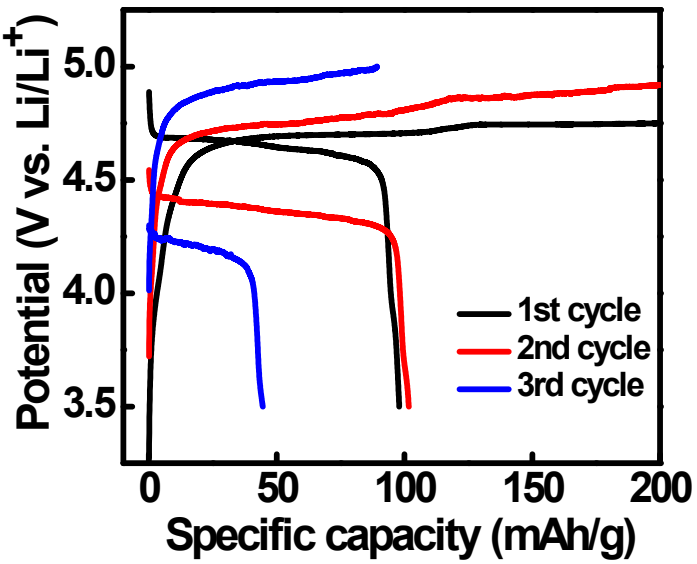

Figure S9. Charge-discharge curves of LNMO cell with 1 M $LiPF_6$/EC:DEC electrolyte recorded at 0.1 C and 55 °C.